Structure of Shock Waves in Bubbly Liquid

AUTHOR(S):

Ishii, Ryuji; Umeda, Yoshikuni; Hashimoto, Takeshi

CITATION:

Ishii, Ryuji ...[et al]. Structure of Shock Waves in Bubbly Liquid. Memoirs of the Faculty of Engineering, Kyoto University 1994, 56(4): 147-175

ISSUE DATE:

1994-10-31

URL:

http://hdl.handle.net/2433/281497

Structure of Shock Waves in Bubbly Liquid

by

Ryuji Ishii*, Yoshikuni Umeda* and Takeshi Hashimoto**

(Received July 5, 1994)

Abstract

In this paper, steady and unsteady shock waves in a bubbly liquid are treated numerically. A new system of model equations describing the bubbly flow is applied and the detailed flow structure behind a shock front is investigated in detail. It is proved that the velocity difference between the liquid and the gas phases induced by a stationary shock wave is of order $\alpha^{1/2}$, wher α is the void fraction of the gas-phase. Radial oscillation of bubbles tends to produce a oscillatory profile of the translational velocity of the bubbles near the wave fronts. Numerical simulation shows that oscillatory behaviour of the mixture pressure is significantly suppressed by the translational motion of bubbles and that the whole shock structure is remarkably affected by the velocity difference between the phases especially in the case of weak shocks. It is confirmed that the stationary shock wave is realized as an asymptotic solution for a shock tube problem with uniform conditions in the low pressure and high pressure chambers.

1. Introduction

The problem of propagation of shock waves through a bubbly liquid has received considerable attention. The speed of a shock wave propagating through a liquid containing small gas bubbles was first studied theoretically and experimentally by Campbell and Pitcher[1]. It was shown that the shock front is very thin and that the pressure of the mixture is strongly oscillatory behind the strong shock front. The speed of the shock wave depends on the shock strength and the void fraction of the gas-phase. Eddington[2] investigated steady shock waves in a gas-liquid mixture, where it was found that the pressure jump across the shock is well predicted with a theory under the isothermal assumption. Later, Crespo[3] investigated the shock structure analytically with some simplifying assumptions. Noordzij[4] and Noordzij & Wijngaarden[5] performed experiments of shock propagation in a bubbly liquid and found that there are three types of shock structure. They also confirmed analytically that the shock structure depends on the shock strength. Tan & Bankoff[6] considered theoretically the effects of relative translational motion of bubbles. However, in their

*Division of Aeronautics and Astronautics, Department of Engineering Science
**Toyota Motor Cooporation, Toyotacho, Toyotashi 471

numerical simulation, the velocity difference is neglected and then a quantitative discussion on the importance of the velocity difference was not given.

Recently Ivandaev[7] performed numerical simulations and found that the thermal conduction between the liquid and gas phases is very important for attenuation of radially oscillatory motion of bubbles, which is consistent with the experimental observation. However, in his analysis it is assumed that the volocity difference between the two-phases is negligible. Beylich & Gülhan[8] performed systematic numerical simulation and experiment of shock waves in bubbly liquid and obtained good agreement between them. In their analysis, however, the effects of the velocity difference between the two-phases are neglected and a few empirical parameters are introduced to fit the numerical results to the experiments.

In many previous papers, the effects of the velocity difference between the two phases on the stationary shock waves are assumed to be negligible. This assumption is not always appropriate. Although in general the thermal dissipation plays the most important role in determining the shock stucture, the effect of the relative translational motion of the bubbles can not be neglected, especially for weak shock waves. This is because any shock is responsible for a finite value of the induced velocity of the mixture far downstream of the shock. In the relaxation region, velocities of the two phases are different and then the adjustment process of the velocity difference due to the drag force, determines the total length of the relaxation region. Dispersion and dissipation processes associated with the expanding and contracting motions of bubbles usually affect the shock structure in the region near the shock front. These discussions suggest that the shock structure cannot be determined precisely without considering the effect of the velocity difference between the two phases.

It is also important to point out that, strictly speaking, stationary shock waves cannot be realized experimentally, owing to the presence of gravitational force. The buoyance force is always responsible for the rising motion of bubbles in the liquid. In the experiment in a vertical shock tube, the rising velocity of the bubbles may be much larger than the bubble velocity induced by the shock wave. Moreover, the mixture pressure always changes along the shock tube owing to the gravitational force and further even the initial conditions are not uniform both in the high and the low pressure chambers. In such a situation, we can never expect to realize any stationary shock. Only in the cases of a mixture composed of gas bubbles and a liquid with very large viscosity, can we use a horizontal shock tube and get the uniform initial conditions necessary to realize a stationary shock wave. Practically, however, the mixture composed of gas bubbles and a highly viscous liquid is a rather extreme example. Theoretical analysis of unsteady shock waves is, therefore, inevitable for precise discussion or evaluation of experimental results in the vertical shock tube.

In the present paper, a new system of model equations describing the bubbly flow proposed previously[9] is applied for the analysis of weak shock waves. First, stationary shock waves in a bubbly liquid are treated. The detailed flow structure behind a shock front and the effect of the velocity difference between the two phases on the shock structure is investigated numerically. Numerical simulation will show that oscillatory behaviour of the mixture pressure is significantly affected by the relative translational motion of bubbles. Next, the shock tube problems are treated and the unsteady behavior of the shocks is discussed. It will be confirmed that the stationary shock is definitely obtained as an asymptotic solution to the shock tube problem. All the numerical simulations are performed on a supercomputer Fujitsu VP-2600 in the Data Processing Center of Kyoto University.

2. Basic Equations

2.1 Conservation equations

We consider a one-dimensional flow of a mixture composed of an incompressible liquid with small gas bubbles dispersed in it. It is assumed that the bubbles remain spherical throughout the flow, have locally uniform size and do not breakup or coalesce ; that the pressure within each bubble is uniform ; that no phase change takes place ; and that the temperature of the liquid remains constant throughout the flow.

Under these assumptions, the governing equations for a one-dimensional unsteady flow are given as[9]

$$\frac{\partial}{\partial t}(1-\alpha)+\frac{\partial}{\partial x}[(1-\alpha)u_l]=0, \tag{1}$$

$$\frac{\partial}{\partial t}(\rho_g\alpha)+\frac{\partial}{\partial x}(\rho_g\alpha u_g)=0, \tag{2}$$

$$\frac{\partial}{\partial t}[(1-\alpha)u_l]+\frac{\partial}{\partial x}[(1-\alpha)u_l^2+p]=0, \tag{3}$$

$$\frac{Du_g}{Dt}+\frac{\varepsilon}{k\tau}\frac{D_g}{Dt}(k\tau)-\left(1+\frac{1}{k}\right)\frac{Du_l}{Dt}+\frac{D_M}{k\alpha}\frac{\partial}{\partial x}(\alpha\rho_g)+\frac{H}{k\alpha}\frac{\partial}{\partial x}\left(\frac{D_g\alpha}{Dt}\right)$$
$$=-\frac{9}{Re}\frac{\varepsilon}{kR^2}, \tag{4}$$

where

$$\tau=\frac{1}{\rho_g}=R^3 \tag{5}$$

$$\varepsilon = u_g - u_l \tag{6}$$

$$k = \frac{1}{2}(1+\lambda\alpha), \tag{7}$$

and

$$\frac{D_g}{Dt} = \frac{\partial}{\partial t} + u_g \frac{\partial}{\partial x}, \quad \frac{D_l}{Dt} = \frac{\partial}{\partial t} + u_l \frac{\partial}{\partial x}. \tag{8}$$

Here the time t, the space coordinate x, the fluid velocity u, the pressure p, the gas density ρ_g, the bubble radius R, and the coefficients of diffusion force and replusive force, D_M and H, are nondimensionalized by R_0/U_0, R_0, U_0, $\rho_l U_0^2$, ρ_{g0}, R_0, $(4/3)\pi R_0^3 \rho_l U_0^2$, $R_0 U_0$, respectively, where U_0 is a reference velocity. The subscript zero denotes the uniform flow conditions ahead of the shock front and the subscripts g and l denote the gas phase and the liquid phase, respectively. The parameter λ in the added mass coefficient of a spherical bubble k in Eq. (7) is given by Wijngaarden[10] as $\lambda = 2.78$. The bubble Reynolds number in Eq. (4) is defined by

$$Re = \frac{\rho_l U_0 R_0}{\mu_l}. \tag{9}$$

The parameters D_M and H, first introduced by Batchelor[11], are quantities that can be determined, at least in principle, from the detailed study of hydrodynamic interactions between bubbles. Unfortunately, these forces have not yet been evaluated theoretically. However, these parameters mainly affect the hyperbolicity of the system, but do not affect appreciably the main flow properties[9]. In the following analysis, therefore, D_M and H are assumed to be small positive constants.

2.2 Equations of expanding motion of bubbles and of the state of the gas.

Since the gas inside each bubble is compressible, two more equations are needed to close the system. These are the momentum equation for radial motion of each bubble and the equation for the state of the gas inside the bubble. The first is given in the nondimensional form as

$$p_g - p = R\frac{D_g^2 R}{Dt^2} + \frac{3}{2}\left(\frac{D_g R}{Dt}\right)^2 + \frac{4\Psi}{Re}\cdot\frac{1}{R}\frac{D_g R}{Dt}, \tag{10}$$

which is the so-called Rayleigh-Plesset equation, where the parameter Ψ is a correction factor due to the dissipation processes in the gas and the liquid phases.

The second is given by

$$p_g=\Gamma\rho_g{}^n \tag{11}$$

where n is an effective polytropic exponent of the gas. The nondimensional parameter Γ is defined by

$$\Gamma=\frac{p_0}{\rho_l U_0{}^2}. \tag{12}$$

Strictly speaking, the gas temperature and the density inside the bubble are not uniform even under the reasonable assumption of uniform gas pressure[12]. But to make the problem tractable numerically, some averaging of the gas density over each bubble is inevitable. This averaging process is closely connected to the evaluation of the thermal damping. The thermal damping is introduced by considering the temperature field of the gas inside a bubble. Such an analysis has been given, for example, by Prosperetti[12]. His result can be incorporated with the equation for the state of the gas, Eq. (11), to the first approximation by putting

$$n=1+\frac{ln[1+\Theta_I(X)]}{ln\rho_g},\quad \Theta_I=\frac{(\gamma-1)}{15\gamma D}-\rho_g{}^{-2/3}\frac{D_g\rho_g}{Dt} \tag{13}$$

for a nearly isothermal shock, and

$$n=\gamma+\frac{ln[1+\Theta_A(X)]}{ln\rho_g},\quad \Theta_A=\frac{3\gamma}{4\pi}D\int_0^z[\rho_g(z-s)^{-(\gamma-1)}-1]\frac{ds}{s^{1/2}} \tag{14 a}$$

$$z=(4\pi)^2\int_0^t\rho_g{}^{(\gamma-4/3)}(t')\,dt',\quad t=\frac{x}{U_s} \tag{14 b}$$

for a nearly adiabatic shock, wher

$$D=\frac{\chi_g}{R_0U_0},\quad \chi_g=\frac{\varkappa_{g0}}{\rho_{g0}C_{pg}}. \tag{15}$$

Here χ_g and $\varkappa_g$ are the thermal conductivity and diffusivity of the gas, respectively and C_{pg} is the specific heat at constant pressure. In the nearly isothermal and adiabatic cases, the gas density ρ_g in the above equations is defined as an averaged density over the bubble. Obviously, the parameter n is not constant and changes its value throughout the flow.

Since the shock wave has a finite strength, the flow conditions upstream of the shock front are different from those far downstream of the shock. It is reasonable to expect that the gas phase will behave nearly adiabatically near the shock front ($n \sim \gamma$) but nearly isothermally far downstream ($n \sim 1$). Then neither of Prosperetti's results, Eq. (13) and Eq. (14), can be applied to the whole flow region. It has to be stressed that the shock structure cannot be analyzed separately but the whole flow region must be solved simultaneously. In light of this, in the present paper n is approximated to be a constant in the range from 1 to γ, and moreover, as in the analysis of Noordzij & Wijngaarden[5], the damping factor Ψ in Eq. (10) is approximated to be a constant given by the linear analysis of Devin[13] as

$$\Psi=1+\psi_R+\psi_T,\ \psi_R=\frac{\delta_R}{\delta_V},\ \psi_T=\frac{\delta_T}{\delta_V} \tag{16}$$

wher δ_V, δ_R and δ_T are the damping factors due to the liquid viscosity, the acoustic radiation by bubbles in the liquid and the thermal dissipation in the gas, respectively. These are given by

$$\delta_V=\frac{4\mu_l\omega}{3np_r},\ \delta_R=\frac{R_r}{C_l}\omega,\ \delta_T=\frac{3(\gamma-1)}{\sqrt{2}}\left(\frac{\mu_g}{\rho_{gr}\mathrm{Pr}_g}\right)^{1/2}\frac{1}{\omega^{1/2}R_r} \tag{17}$$

where the subscript r denotes some reference conditions and ω is the resonant frequency of a bubble defined by

$$\omega^2=\frac{3np_r}{\rho_l R_r{}^2}. \tag{18}$$

In these equations, μ is the viscosity, C_l the speed of sound in the liquid and Pr_g the Prandtl number of the gas.

Strictly Eqs. (16-18) cannot be applied with sufficient accuracy to any nonlinear shock wave with a finite strenght. Of course, we can solve the temperature field within a bubble exactly as in the Prosperetti's paper[12] for a spherical bubble. However, the sphericity of the bubble itself is an approximation. For a deformable bubble, it will be very difficult to determine the temperature field even numerically. In the present study, only weak shocks (with pressure ratios less than 1.15) are treated and attention is mainly paid to the ffects of translational velocity slip between the two phases. Such a situation will, therefore, justify the use of Eq. (16) in conjunction with Eqs. (17) and (18) as a damping factor and of Eq. (11) with a constant effective polytropic exponent n in the range from 1 to γ, at least for

qualitative discussions.

Here it will be worthwhile to point out that Prosperetti's result yields a thermal damping factor similar to Eq. (16). For the nearly isothermal shock (D≫1), Eqs. (10) is not substantially affected by rewriting Eq. (11) and (13) as

$$p_g=\rho_g \quad (n=1) \tag{19}$$

$$\Psi=\Psi'+\phi_T, \text{ where } \phi_T=\frac{\Gamma(\gamma-1)}{20\gamma}\frac{Re}{D}\rho_g{}^{4/3} \tag{20}$$

In this case, the damping factor Ψ' should include only the contributions from the viscousity and the acoustic radiation, and then Ψ' can be put to $\Psi'=1+\phi_A$.

3. Stationary Shock Waves

3.1 Numerical scheme

For stationary shock waves, the coordinate system (t, x) is transformed into (ξ, η) by

$$\xi=x+U_st, \ \eta=t \tag{21}$$

where U_s is the speed of shock wave defined later. After straightforward but lengthy manipulation, Eqs. (1) to (4), Eqs. (10) and (11) in conjunction with Eqs. (5) to (7) are rearranged by making use of the relation $\partial(\ )/\partial\eta=0$ to yield

$$\frac{1}{\beta}\frac{d\beta}{d\xi}+\frac{1}{\rho_g}\frac{d\rho_g}{d\xi}-\frac{\varepsilon}{U_s}\beta\rho_g\left(\frac{\lambda\alpha_0}{1+\lambda\alpha_0\beta}\frac{d\beta}{d\xi}-\frac{1}{\rho_g}\frac{d\rho_g}{d\xi}\right)$$
$$+\alpha_0\left(1+\frac{1}{k}\right)\beta^2\rho_g{}^2\frac{(1-\alpha_0)^2}{(1-\alpha_0\beta)^3}\frac{d\beta}{d\xi}-\frac{9}{ReKU_s}\beta^2\rho_g{}^{8/3}\frac{\varepsilon}{U_s}=0 \tag{22}$$

$$\frac{d^2\rho_g}{d\xi^2}-\frac{17}{6}\frac{1}{\rho_g}\left(\frac{d\rho_g}{d\xi}\right)^2-\frac{1}{\beta}\frac{d\beta}{d\xi}\frac{d\rho_g}{d\xi}+\left(\frac{4\Psi}{ReU_s}\right)\beta\rho_g{}^{5/3}\frac{d\rho_g}{d\xi}+\frac{3\Gamma}{U_s{}^2}\beta^2\rho_g{}^{11/3}\frac{\Delta p}{\Gamma}=0 \tag{23}$$

$$u_g=U_s\left(\frac{1}{\beta\rho_g}-1\right) \tag{24}$$

$$u_l=U_s\frac{\alpha_0(\beta-1)}{(1-\alpha_0\beta)} \tag{25}$$

$$p=\Gamma-U_s{}^2\alpha_0(1-\alpha_0)\frac{(\beta-1)}{(1-\alpha_0\beta)} \tag{26}$$

$$p_g=\Gamma\rho_g{}^n \tag{27}$$

where

$$\beta=\frac{\alpha}{\alpha_0}, \tag{28}$$

$$\frac{\varepsilon}{U_s}=\frac{u_g-u_l}{U_s}=\frac{1-\beta\rho_g}{\beta\rho_g}+\alpha_0\frac{1-\beta}{1-\alpha_0\beta} \tag{29}$$

$$\begin{aligned}\frac{\Delta p}{\Gamma}=\frac{p_g-p_l}{\Gamma}&=\rho_{gn}-\frac{(1-\alpha_0)(\beta_1-\beta)}{(1-\alpha_0\beta)(\beta_1-1)}-\frac{(1-\alpha_0\beta_1)(\beta-1)}{(1-\alpha_0\beta)(\beta_1-1)}\rho_{g1n}\\&=\rho_{gn}-1+\frac{\rho_{g1}(1-\rho_{g1n})}{(1-\rho_{g1})}\frac{\beta-1}{(1-\alpha_0\beta)}\end{aligned} \tag{30}$$

$$\begin{aligned}U_s^2&=\frac{\Gamma(1-\alpha_0\beta_1)}{\alpha_0(1-\alpha_0)(\beta_1-1)}\left\{1-\left[\frac{1-\alpha_0\beta_1}{(1-\alpha_0)\beta_1}\right]^n\right\}\\&=\frac{\Gamma}{\alpha_0(1-\alpha_0)}\frac{\rho_{g1}(1-\rho_{g1n})}{(1-\rho_{g1})}.\end{aligned} \tag{31}$$

The above system is subject to the boundary conditions

$$\begin{aligned}&u_g=u_l=0,\ \rho_g=1,\ \alpha=\alpha_0,\ p=p_g=\Gamma && \text{at } x=-\infty,\\&u_g=u_l,\ \rho_g=\rho_{g1},\ \alpha=\alpha_1,\ p=p_g=\Gamma\rho_{g1n} && \text{at } x=\infty,\end{aligned} \tag{32}$$

Numerically the shock front is assumed to be located at $x=0$. The subscript 1 denotes flow conditions far downstream of the shock. In these equations, the diffusion and the repulsive forces are neglected. This is because the steady solution is free from ill-posedness of the system as an initial value problem and moreover these forces do not affect appreciably the flow properties. Later, a more quantitative discussion about the effects of these forces will be given.

For the existence of stationary shock waves, ρ_{g1} must be greater than ρ_{g0} $(=1)$. Since the detailed discussions about the locus of solution curves near the shock front and the downstream boundary in the phase plane is given in Refs. 3, 6 and 8, we will not dwell on this problem any more here.

Since Eqs. (22) and (23) in conjunction with Eqs. (28) to (31) constitute a system of simultaneous ordinary differential equations for β and ρ_g, they can be solved for the boundary conditions (32). Once these are solved, the solution can be substituted into Eqs. (24) to (27) to determine u_g, u_l, p and p_g.

Before proceeding to the numerical simulation, we will derive some important information analytically from the above equations in the case of the small void fraction α_0. From Eq. (31), we have

$$U_s=O(\alpha_0^{-1/2}), \tag{33}$$

with which Eq. (22) in conjunction with Eq. (29) yields

$$\beta\rho_g=1+O(\alpha_0). \tag{34}$$

When this is substituted into Eq. (29) again, we get

$$\varepsilon=u_g-u_l=O(\alpha_0^{1/2}). \tag{35}$$

In many previous papers, the velocity difference has been neglected as a small quantity of order α_0. Obviously this is not the case. For example, $\alpha_0^{1/2}=0.1$ for $\alpha_0=0.01$, and further the velocity difference for $\alpha_0=0.01$ is not always small and so cannot be neglected as in Refs. 2, and 6 to 8. This is one of the most important results in this paper. Our numerical results will support this result.

Table 1 Physical constants for $p_0=1.0135\times10^5$ N/m², $T_0=15.0$ ℃

Air	Water
$\rho_{g0}=1.23$ kg/m³	$\rho_l=1.0\times10^3$ kg/m³
$C_{pg}=1.006\times10^3$ J/kg. K	$\mu_l=1.002\times10^{-3}$ kg/m. s
$\gamma=1.4$	$C_l=1.5\times10^3$ m/s
Prg=0.72	
$\mu_g=1.78\times10^{-5}$ kg/m. s	
$\kappa_g=2.41\times10^{-2}$ J/m. s. K	

3.2 Results and discussions

In what follows, numerical simulations are performed for a bubbly liquid composed of air and water. The physical constants are listed in Table 1, where T_0 is the temperature of the undisturbed mixture. The reference velocity U_0 is put to 10 m/s so as to make the parameter Γ order unity for analytical and numerical convenience.

The fourth-order Runge-Kutta-Gill method was adopted for the numerical simulation of stationary shock waves. Undisturbed flow conditions for the air-water mixture are $p_0=1.013\times10^5$ N/m², $T_0=15$ ℃, $\alpha_0=0.05$, $R_0=0.5$ mm. The shock strength is controlled by specifying the pressure ratio p_1/p_0 and the effective

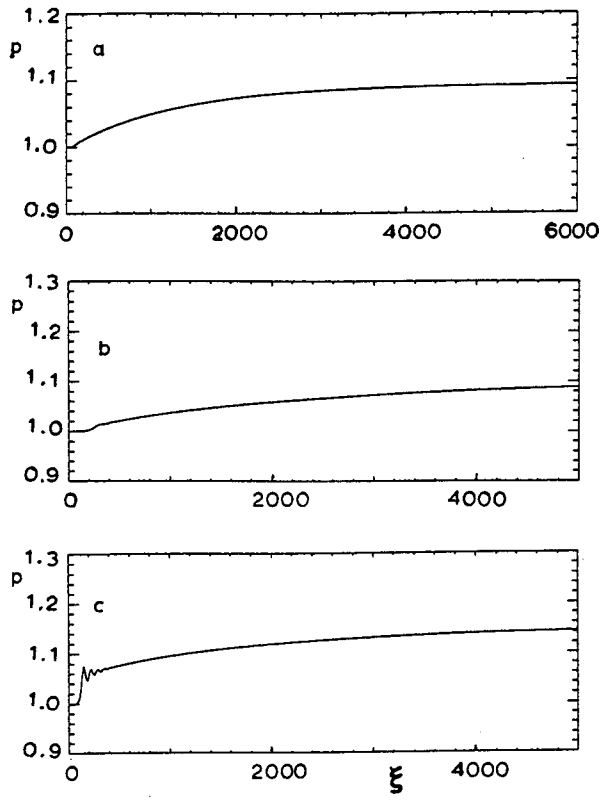

Fig. 1 Stationary shock waves for $n=1.0$: a $p_1/p_0=1.0933$, b $p_1/p_0=1.1$, c $p_1/p_0=1.15$.

polytropic exponent n.

In Fig. 1, pressure profiles are shown for $p_1/p_0=1.0933$, 1.10 and 1.15. for $n=1.0$, where the damping coefficients Ψ evaluated from Eq. (16) in conjunction with Eqs. (17) and (18) for $p_r=(p_0+p_1)/2$, $\rho_{gr}=(\rho_{g0}+\rho_{g1})/2$, and $R_r=(R_0+R_1)/2$ are 115.3, 115.1 and 114.4, respectively. The shock speeds U_s in m/s for these three shocks are 48.29, 48.43 and 49.52, respectively. These show three type of flow patterns as first found experimentally by Noordzij & wijngaarden[5]. Profiles of the pressure, the velocities and the void fraction are shown in Fig. 2 for $p_1/p_0=1.11$.

In many previous studies, the velocity slip $\varepsilon=u_g-u_l$ is set to zero, because the effects of ε on the structure was assumed to be negligible. As stated previously, however, this is never the case. To prove this, the correspoding shocks for the mixture model are calculated by replacing Eq. (22) by $u_g=u_l$ or

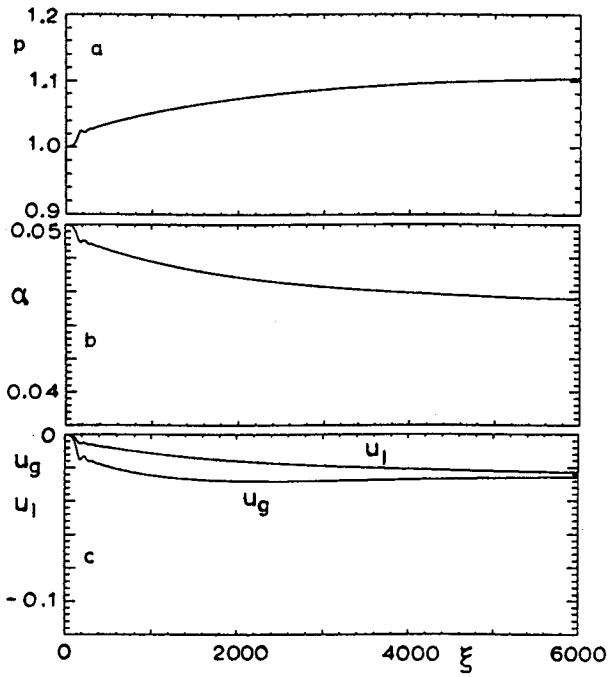

Fig. 2 Shock structure of a stationary shock for $p_1/p_0=1.11$ and $n=1.0$; a pressure, b void fraction, c bubble and liquid velocities.

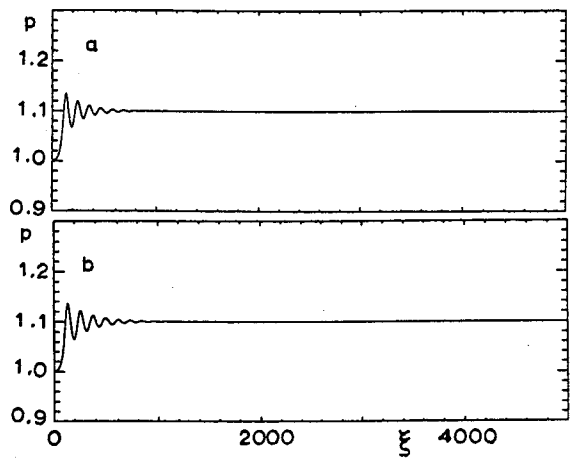

Fig. 3 Effect of effective polytropic exponent n; a $n=1.0$, $p_1/p_0=1.1$, b $n=\gamma(=1.4)$, $p_1/p_0=1.1$.

$$\alpha=\frac{\alpha_0}{(1-\alpha_0)\rho_g+\alpha_0}. \tag{36}$$

The results are shown in Fig. 3a for $p_1/p_0=1.1$ and $n=1.0$. Obviously, the difference between the shocks in Figs. 1b and 3a is remarkable. The effect of velocity difference ε is locally very small but it is cumulative. The whole shock structure must be determined simultaneously and then the cumulative effect becomes important. Owing to the relative translational motion of bubbles, the pressure oscillation and the peak pressure near the shock front are effectively suppressed and the shock layer is also remarkably elongated.

Using Eq. (22) in conjunction with Eq. (29), the shock thickness d can be roughly estimated to be $d \sim ReU_sk/9$. For the shocks considered here, the shock thickness is about 1200. Since the reference length R_0 was taken to be 0.5 mm, the shock thickness d is about 0.6 m, which is much less than the numerical results shown in Figs. 1 and 2. This may come from the fact that the shock in the bubbly liquid is not

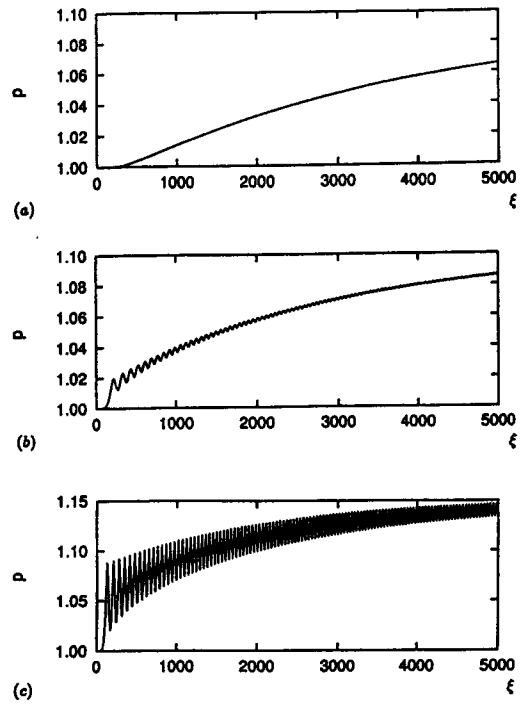

Fig. 4 Pressure distributions for $\Psi=1.0(\psi_R=\psi_T=0.0)$; a $p_1/p_0=1.085$, b $p_1/p_0=1.11$, c $p_1/p_0=1.15$.

only dissipative but also dispersive. Further, the shock thickness or the shock structure cannot be estimated by the viscous dissipation only. Empirically the shock thickness d was found to be estimated by $d=ReU_sk/9\ \alpha_0^{1/2}$ which yields $d \sim 3$ m for the present cases and is quite consistent with the results in Figs. 1 and 2[4].

To investigate the effect of the polytropic exponent n, a shock for the mixture model is shown in Fig. 3b for $n=1.4$ and $p_1/p_0=1.1$. Obviously the main features are very similar to the shock in Fig. 3a. It was confirmed that in general the value of n put to a constant does not affect the flow pattern at all, but affects the shock speed and the frequency of pressure oscillation near the shock front. This means that the flow pattern depends mainly on the pressure ratio p_1/p_0 and the damping factor Ψ.

It has been pointed out that the effect of the thermal dissipation is of primary importance for the atenuation of the bubble oscillation. In order to investigate this situation, the pressure profiles are shown in Figs. 4a to 4c for $p_1/p_0=1.085$, 1.10 and 1.15, respectively, where the dissipations due to the thermal conduction and the acoustic radiation are neglected ($\Psi=1.0$). The corresponding results for $\Psi=1.0+\psi_R$

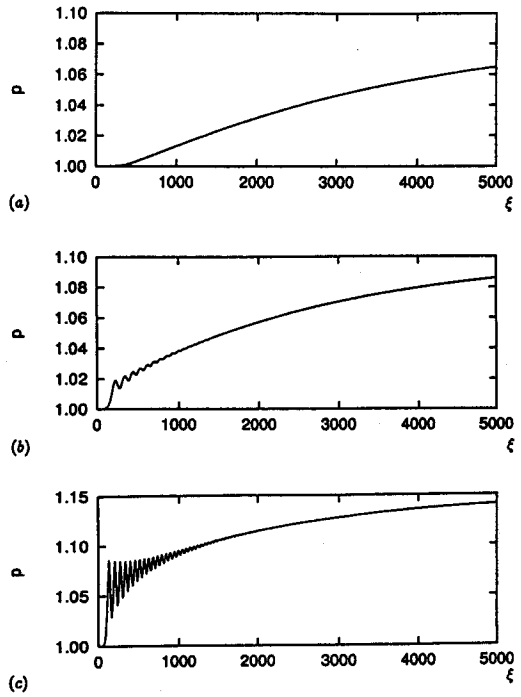

Fig. 5 Pressure distributions for $\Psi=1.0+\psi_R(\psi_T=0.0)$; a $p_1/p_0=1.085$, b $p_1/p_0=1.11$, c $p_1/p_0=1.15$.

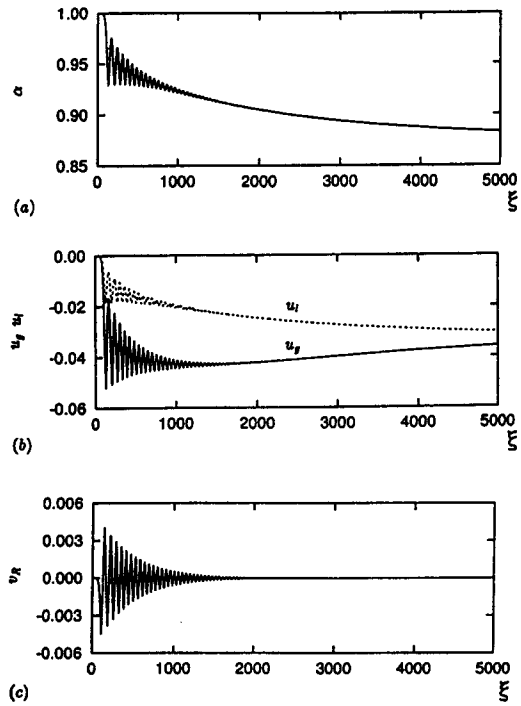

Fig. 6 Distributions of void fraction α, bubble belocity u_g, liquid velocity u_l, and expanding velocity of bubbles v_R for $p_1/p_0=1.15$ and $\Psi=1+\psi_R$.

are shown in Figs. 5a to 5c, where only the thermal dissipation is neglected. Comparison among the results in Figs. 1, 4 and 5 suggests that the thermal dissipation plays the most important role in the suppresion of the oscillatory behavior of the mixture pressure. It has to be stressed, however, that the pressure profile for $p_1/p_0=1.085$ is not appreciably affected by the thermal and acoustical dissipation. This means that the structure of weak shock waves is mainly controlled by the viscous drag due to the velocity difference between the two phases.

Obviously the bubble oscillation is important for relatively strong shocks as shown in Figs. 4 and 5. In Figs. 6a to 6c, distributions of the void fraction α, the bubble velocity u_g, liquid velocity u_l and the expanding velocity of the bubble v_R are shown for $p_1/p_0=1.15$ and $\Psi=1+\psi_R$. This shows that the bubbles oscillate significaltly near the shock front. This oscillation is responsible for the pressure oscillation as shown in Fig. 5c. Compared with the result in Fig. 1c, the pressure oscillation is remarkably enhanced without the thermal dissipation. In spite of this,

it is interesting that the average or the global behavior of the shock layer is almost independent of the thermal and acoustical dissipations.

4. Unsteady Shock Waves

4.1 Numerical scheme

Next we consider a shock tube problem, where the undisturbed conditions in the low and high pressure chambers are uniform. After a diaphragm separating two chambers is ruptured, compression waves propagate in the low pressure chamber and rarefaction waves propagate in the high pressure chamber. For a single gas-phase flow, such a shock tube problem is well understood analytically, as well as numerically, at least for an ideal gas. But for the bubbly liquid, the situation is quite different. As far as the authors know, there have been no papers treating the shock tube problem of bubbly liquid analytically. This may be accounted for by the important fact that the construction of a system of model equations is very difficult. Mathematically, hyperbolicity or well-posedness of the system is of crucial importance. Fortunately, the governing equations (1-4), in conjunction with Eq. (5-8), constitute a well-posed system as an initial value problem, if the coefficient of the diffusion force D_M is chosen as a small positive constant[9].

Here we apply an Total-Variation-Diminishing (TVD) scheme developed by Chakravarthy & Osher[14], which has proved to be very effective for the numerical analysis of a supersonic gas-particle flow[15]. Although the present system can be a hyperbolic system, the TVD-scheme cannot be applied directly because the momentum equation of bubbles, Eq. (4), is not given in the conservation form, which is essential for the successful application of the TVD-scheme. So some rearrangement of the momentum equation is needed. We rewrite Eqs. (1) to (4) as

$$\frac{\partial q}{\partial t}+\frac{\partial f}{\partial x}=h \tag{37}$$

$$q^T=[(1-\alpha),\ \alpha\rho_g,\ (1-\alpha)u_l,\ k\alpha\varepsilon], \tag{38 a}$$

$$f^T=[(1-\alpha)u_l,\ \alpha\rho_g(u_l+\varepsilon),\ (1-\alpha)u_l^2+\Gamma\rho_{gn},\ k\alpha\varepsilon u_g+n\Gamma\alpha_0\psi+a\rho_g D_M], \tag{38 b}$$

$$h^T=\Big[0,\ 0,\ W,\ -k\alpha\varepsilon\frac{\partial u_l}{\partial x}-\frac{n\Gamma\rho_{gn-2}}{(1-\alpha)}(\alpha\rho_g-\alpha_0+\alpha_0\alpha)\frac{\partial\rho_g}{\partial x}-H\frac{\partial}{\partial x}\Big(\frac{D_g a}{Dt}\Big)$$
$$\frac{\alpha W}{1-\alpha}-\frac{9}{Re}\alpha\rho_g R\varepsilon\Big], \tag{38 c}$$

where

$$\psi=\int \rho_g{}^{n-2} d\rho_g, \tag{39}$$

$$W=\frac{\partial}{\partial x}(p_g-p)=(1-\alpha)\frac{D_l u_l}{Dt}+\frac{\partial p_g}{\partial x}, \tag{40}$$

and the superscript T denotes transpose. In the momentum equation of bubbles, Eq. (4), the relation

$$\frac{\alpha}{1-\alpha}\frac{\partial p_g}{\partial x}=n\Gamma\alpha_0\frac{\partial \psi}{\partial x}+\frac{n\Gamma\rho_g{}^{n-2}}{(1-\alpha)}(\alpha\rho_g-\alpha_0+\alpha_0\alpha)\frac{\partial \rho_g}{\partial x}, \tag{41}$$

was used to get the above rerranged system. In this equation, the first term on the right hand side can be written as $\partial(n\Gamma\alpha_0\psi)/\partial x$ and the second term may be very small at least near the shock front, because $\alpha\rho_g-\alpha_0=0(\alpha_0{}^2)$ as was shown in the previous chapter for the stationary shock waves. We can also get a relation $\partial u_l/\partial x=0(\alpha_0)$ from Eq. (1). From these, it is obvious that the two terms, including the first-order space derivatives in Eq. (38 c), are very small for small α_0. Further although the original momentum equation of bubbles is not given in the conservation form, the rearranged equation can be used to approximate a conservation law in the numerical simulation.

For more precise discussion of the rearranged system, the characteristic speeds ν of the system are obtained from

$$det\,(\mathrm{A}-\nu\mathrm{I})=0, \tag{42}$$

where I is the unit matrix and A is given by $\partial f/\partial p$ as

$$\mathrm{A}=\begin{bmatrix} 0 & 0 & 1 & 0 \\ \rho_g\left(\varepsilon\frac{4k-1}{2k}-\frac{\alpha u_l}{1-\alpha}\right) & \varepsilon+u_l & \frac{\alpha\rho_g}{(1-\alpha)} & \frac{\rho_g}{k} \\ (1-\alpha)C^2-u_l{}^2 & \frac{1}{\rho_g}(1-\alpha)C^2 & 2u_l & 0 \\ \frac{1}{2}\varepsilon^2(4k-1)+\frac{\alpha_0}{\rho_g}(1-\alpha)C^2-\frac{k\alpha\varepsilon u_l}{1-\alpha} & D_M+\frac{\alpha_0}{\rho_g{}^2}(1-\alpha)C^2 & \frac{k\alpha\varepsilon}{1-\alpha} & 2\varepsilon+u_l \end{bmatrix}, \tag{43}$$

where C is the sound speed of the mixture defined by

$$C^2=\frac{n\Gamma p_{g^n}}{\alpha(1-\alpha)}. \tag{44}$$

Eq. (42) is rewritten as

$$X^4+3\varepsilon X^3+\left\{2\varepsilon^2-\frac{\rho_g D_M}{k}-C^2\left[1+\frac{\alpha_0}{k\rho_g}(1-\alpha)\right]\right\}X^2-\varepsilon C^2\left(1+\frac{1-\alpha}{2k}\right)X$$
$$+\frac{1-\alpha}{k}C^2\left(\rho_g D_M-\frac{\varepsilon^2}{2}\right)=0, \tag{45}$$

where $X=u_l-\nu$. The hyperbolicity of the system requires

$$\rho_g D_M-\frac{\varepsilon^2}{2}>0, \tag{46}$$

which is different by order α_0 from the corresponding requirement for the original system[9]. Numerically it was also confirmed that two eigenvalues ν, associated with the pressure waves, and the remaining two associated with the voidage waves obtained from Eq. (45), are different from those of the original system by order α_0^2 and α_0, respectively. It has to be stressed that the system of Eqs. (37) to (40) is mathematically the same as the original system of Eqs. (1) to (7). The approximated eigen-values or the speeds of pressure and voidage waves are used only for numerical convenience.

Before application of the TVD-scheme, one more task remains to be solved. The right hand side of Eq. (37), Eq. (38 c), has terms with a factor W including time derivatives. These must be rewritten in terms of space derivatives.

With Eqs. (1) and (4) in conjunction with Eq. (40), we have

$$\frac{D_g\rho_g}{Dt}=-\frac{\rho_g}{\alpha}\frac{\partial}{\partial x}(u_l+\alpha\varepsilon) \tag{47}$$

$$\frac{D_g{}^2\rho_g}{Dt^2}=-\frac{\rho_g}{\alpha(1-\alpha)}\left(1+\frac{\alpha}{k}\right)\frac{\partial W}{\partial x}-\frac{\rho_g}{\alpha(1-\alpha)^2}\left(1+\frac{\alpha}{k}+\frac{1-\alpha}{2k^2}\right)\frac{\partial\alpha}{\partial x}\cdot W$$
$$+\frac{\rho_g}{\alpha(1-\alpha)}\left(1+\frac{\alpha}{k}\right)\frac{\partial^2 p_g}{\partial x^2}+\frac{\rho_g}{\alpha(1-\alpha)^2}\left(1+\frac{\alpha}{k}+\frac{1-\alpha}{2k^2}\right)\frac{\partial\alpha}{\partial x}\left(\frac{\partial p_g}{\partial x}\right)+\phi \tag{48}$$

where

$$\frac{\alpha}{\rho_g}\phi=-\varepsilon(1-\alpha)\left(3-\frac{1}{2k}\right)\frac{\partial^2 u_l}{\partial x^2}-\varepsilon\frac{\partial^2}{\partial x^2}(\varepsilon\alpha)-\varepsilon^2\left(2-\frac{1}{2k}\right)\frac{\partial^2\alpha}{\partial x^2}+\frac{D_M}{k}\frac{\partial^2}{\partial x^2}(\rho_g\alpha)$$
$$-\frac{\partial}{\partial x}\left[2\varepsilon(1-2\alpha)-\frac{\varepsilon(1-\alpha)}{2k}\right]\frac{\partial u_l}{\partial x}-\frac{\partial}{\partial x}\left[\varepsilon^2\left(2-\frac{1}{2k}\right)\right]\frac{\partial\alpha}{\partial x}$$
$$+\frac{1}{\alpha}\cdot\frac{\partial}{\partial x}(u_l+\alpha\varepsilon)\left[\frac{\partial}{\partial x}(u_l+\alpha\varepsilon)+(1-\alpha)\frac{\partial u_l}{\partial x}+\varepsilon\frac{\partial\alpha}{\partial x}\right]+\left(\frac{\partial\varepsilon}{\partial x}\right)^2$$
$$-\frac{D_M}{k^2}\frac{\partial k}{\partial x}\cdot\frac{\partial}{\partial x}(\rho_g\alpha)+\frac{9}{Re}\cdot\frac{\partial}{\partial x}\left(\frac{\rho_g{}^{2/3}\alpha\varepsilon}{k}\right)$$
$$+\frac{H}{k}\frac{\partial^2}{\partial x^2}\left[(1-\alpha)\frac{\partial u_l}{\partial x}+\varepsilon\frac{\partial\alpha}{\partial x}\right]-\frac{H}{k^2}\left(\frac{\partial k}{\partial x}\right)\frac{\partial}{\partial x}\left[(1-\alpha)\frac{\partial u_l}{\partial x}+\varepsilon\frac{\partial\alpha}{\partial x}\right]. \tag{49}$$

These are substituted into Eq. (10) in conjunction with Eq. (5) to yield

$$p=p_g-a\frac{\partial W}{\partial x}-bW+a\frac{\partial^2 p_g}{\partial x^2}+b\frac{\partial p_g}{\partial x}$$
$$-\frac{11}{18}\frac{\rho_g{}^{-2/3}}{\alpha^2}\left[\frac{\partial}{\partial x}(u_l+\alpha\varepsilon)\right]^2-\frac{4\Psi}{3Re}\frac{1}{\alpha}\frac{\partial}{\partial x}(u_l+\alpha\varepsilon)+\frac{1}{3}\rho_g{}^{-5/3}\phi. \tag{50}$$

This is again substituted into Eq. (40) to yeield

$$a\frac{\partial^2 W}{\partial x^2}+\left(\frac{\partial a}{\partial x}+b\right)\frac{\partial W}{\partial x}+\left(\frac{\partial b}{\partial x}-1\right)W-a\frac{\partial^3 p_g}{\partial x^3}-\left(\frac{\partial a}{\partial x}+b\right)\frac{\partial^2 p_g}{\partial x^2}-\left(\frac{\partial b}{\partial x}\right)\frac{\partial p_g}{\partial x}$$
$$+\frac{11}{9}\frac{\rho_g{}^{-2/3}}{\alpha^2}\frac{\partial}{\partial x}(u_l+\alpha\varepsilon)\cdot\frac{\partial^2}{\partial x^2}(u_l+\alpha\varepsilon)+\frac{4\Psi}{3Re}\frac{1}{\alpha}\frac{\partial^2}{\partial x^2}(u_l+\alpha\varepsilon)$$
$$+\frac{11}{18}\frac{\partial}{\partial x}\left(\frac{\rho_g{}^{-2/3}}{\alpha^2}\right)\cdot\left[\frac{\partial}{\partial x}(u_l+\alpha\varepsilon)\right]^2-\frac{4\Psi}{3Re}\frac{1}{\alpha^2}\frac{\partial\alpha}{\partial x}\cdot\frac{\partial}{\partial x}(u_l+\alpha\varepsilon)$$
$$-\frac{1}{3}\frac{\partial}{\partial x}(\rho_g{}^{-5/3}\phi)=0, \tag{51}$$

where

$$a=\frac{\rho_g{}^{-2/3}}{3\alpha(1-\alpha)}\left(1+\frac{\alpha}{k}\right),\quad b=\frac{\rho_g{}^{-2/3}}{3\alpha(1-\alpha)^2}\left[1+\frac{\alpha}{k}+\frac{(1-\alpha)}{2k^2}\right]\frac{\partial\alpha}{\partial x} \tag{52}$$

Obviously Eq. (51) is a second order partial differential equation for W with respect to x. Mathematically if the spatial distribution of flow quantities is given, the quantity W is obtained as a solution to Eq. (51) for the appropriate boundary conditions far upstream and far downstream of the wave region.

Now we summarize the numerical procedure:

i) For specified initial conditions at $t=0$, the distribution of W is solved numerically with Eq. (51). The boundary conditions for W are $W=0$ in the regions outside the wave. A Successive-Over-Relaxation (SOR) method is used in the present paper.

ii) With the solved W, all terms in the right hand side of Eq. (37), Eq. (38 c), are calculated for the specified conditions.

iii) Finally the TVD-scheme is applied to determine α, ρ_g, u_l and u_g, which are substituted into Eq. (11) and Eq. (50) to evaluate p_g and p, respectively, at time $t=\Delta t$, where Δt is a small time increment satisfying the Courant-Friedrichs-Levy (CFL) condition,

$$\Delta t < \frac{\Delta t}{C+|u_g|} \tag{53}$$

In this TVD-scheme, Eq. (45) is solved numerically by a modified Bairstow method to get the four eigenvalues ν, which are used to evaluate the right and left eigenvectors given in Appendix A. The accuracy of the TVD-scheme is second-order in space and time.

iv) The procedured (i)-(iii) are repeated to get a solution at any specified time t. As described above, one time-step requires many computations and further one run requires much computing time even on the supercomputer.

For comparison, a numerical solution for the mixture model was also obtained by a similar method. In this case, Eq. (4) is replaced by Eq. (36) and then Eqs. (1) to (3), (5) to (7), (10) and (11) in conjunction with Eqs. (16) and (17) constitute a closed system, which can be solved relatively easily (see Appendix B).

In the shock tube problem, the initial flow conditions in the high and the low pressure chambers separated by a diaphragm must be specified. These are specified as follows;

$$u_l=u_g=0,\ \alpha=\alpha_0,\ \rho_g=1,\ p=p_g=\Gamma, \quad \text{in the low pressure chamber,} \tag{54 a}$$

$$u_l=u_g=0,\ \alpha=\alpha_2,\ \rho_g=\rho_{g2},\ p=p_g=p_2, \text{ in the high pressure chamber,} \tag{54 b}$$

where the diaphragm is located at $x=0$ and the subscript 2 denotes the high pressure chamber. The conditions denoted by the subscript zero are the same as those used in the calculation of stationary shocks. Since the initial states are assumed to be in thermal equilibrium and the temperature is uniform throughtut the whole initial flow region in both the high and low pressure chambers, we consider two cases,

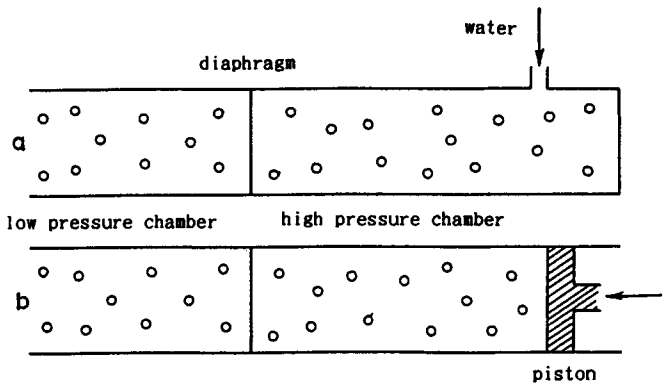

Fig. 7 Initial conditions for shock-tube problem.

$$p_2=\Gamma\rho_{g2},\ \alpha_2=\alpha_0/\rho_{g2}, \tag{55}$$

$$p_2=\Gamma\rho_{g2},\ \alpha_2=\frac{\alpha_0/\rho_{g2}}{(1-\alpha_0)+\alpha_0/\rho_{g2}}. \tag{56}$$

First both chambers are occupied by the same mixture in the conditions described by the subscript zero. After the two chambers are separated by a diaphragm, some water is introduced slowly into the high pressure chamber to get the pressure p_2 as in Fig. 7a. In this case, we have the first condition (55). If after the diaphragm is introduced, a piston located at the end of the high pressure chamber is pushed slowly into the chamber as in Fig. 7b, we have the second condition (56). Since the initial void fraction is chosen to be 0.05, the difference between the two conditions is very small, and it was confirmed that the numerical results do not appreciably depend on the conditions.

4.2 Results and discussions

First of all, it was confirmed that no flow property is appreciably affected by the values of D_M and H in the ranges $0.002<D_M<0.05$ and $0\leqq H<0.01$, respectively, just as in Ref. 9. All the numerical results shown later are for $p_0=1$ atm, $\alpha_0=0.05$, $R_0=0.5$ mm, $D_M=0.01$ and $H=0.001$.

It is interesting to investigate the distribution of an initial discontinuity just after the rupture of a diaphragm. In Fig. 8, a time history of the pressure profile is shown for $p_2/p_1=1.2$ and $n=1$. The pressure is slightly oscillatory near the shock front but it is relatively much more oscillatory behind the rarefaction waves. This may come from the fact that the sharp increase in pressure at the shock front produces a strong

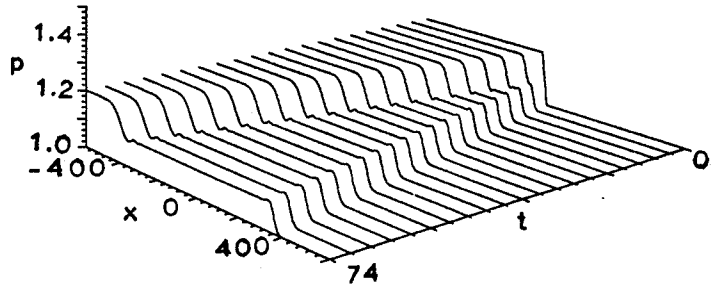

Fig. 8 Time history of pressure profile for $p_2/p_1=1.2$ and $n=1.0$.

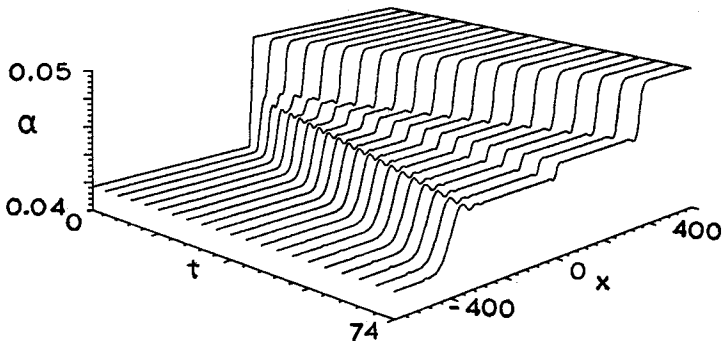

Fig. 9 Time history of void-fraction profile for $p_2/p_0=1.2$ and $n=1.0$.

contraction and acceleration of bubbles which results in effective dissipation. The corresponding result for the void fraction α is shown in Fig. 9. Near the shock front, the void fraction is much more oscillatory than that of the pressure. As in the case of the shock tube problem of an ideal gas, a contact surface is clearly seen in this figure. As was discussed by Prosperetti & Wijngaarden[16], the so-called Riemann invariants do not exist in the bubbly liquid and these wave profiles are not self-similar.

Closer investigation of unsteady waves, profiles of the pressure, the void fraction, the bubble velocity and the liquid velocity are shown in Figs. 10a to 10d, respectively. First, we can see that the slope of the rarefaction waves gradually flattened with time. This is consistent with the experiment of Campbell & Pitcher[1]. Second, the whole wave region is unsteady and the shock front is decaying with time. The rate of decay is however very small. Third, the wavy oscillation of the void fraction near the shock front is appreciably suppressed with time, but the situation is completely

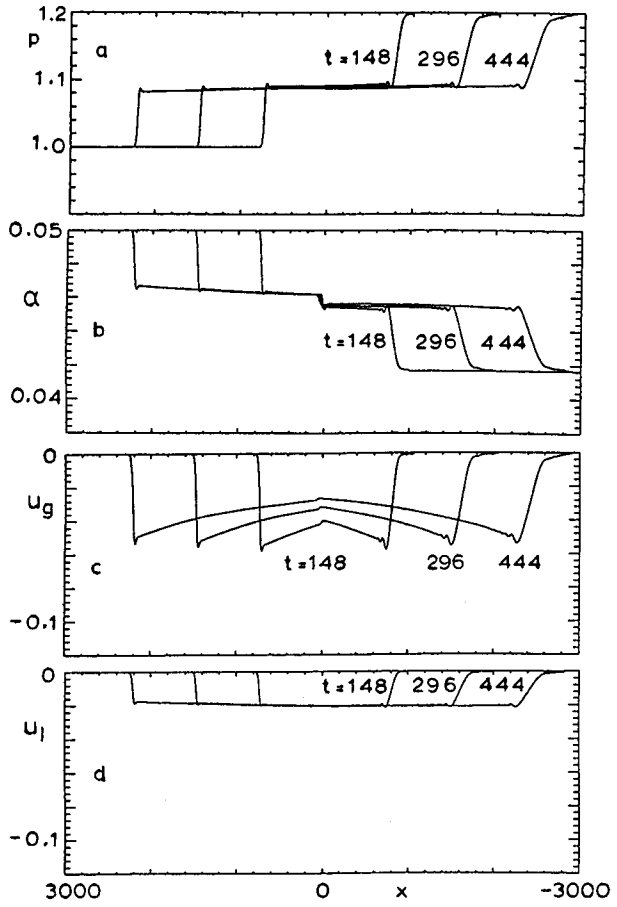

Fig. 10 Time evolution of flow field after rupture of a diaphragm for $p_2/p_0=1.2$, $n=1.0$; a pressure, b void fraction, c bubble velocity, d liquid velocity.

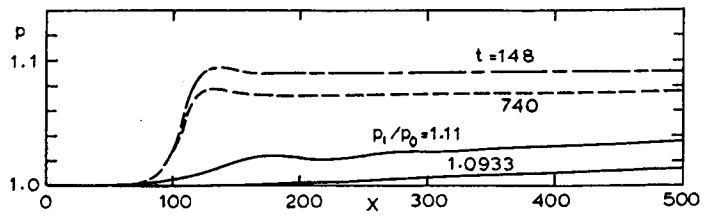

Fig. 11 Time-convergency of shock front for $p_2/p_0=1.2$ and $n=1.0$; —— unsteady shock at $t=148$, ----- unsteady shock at $t=740$, —— stationary shock.

different in the region just downstream of the rarefaction wave. Fourth, the induced bubble velocity is much larger than the liquid velocity[17]. Due to the viscous drag between the two phases, the bubble velocity becomes minimum in its magnitude near the central part of the waves. On the contrary, the magnitude of the liquid velocity becomes maximum near the wave center.

The pressure profiles near the shock front are shown in Fig. 11 and compared with stationary solutions for $p_1/p_0=1.093$ and 1.11 obtained in the previous chapter. Obviously, the unsteady shock is decaying with time and approaching a stationary one. It has to be stressed that we cannot know the pressure ratio p_1/p_0 of the stationary shock which the unsteady shock approaches asymptotically. Only when the asymptotically time-converged solution is obtained, the flow conditions denoted by the subscript 1 are found for the specified conditions in the high pressure chamber denoted by the subscript 2. In the present case, however, the relaxation region of the velocity difference $\varepsilon=u_g-u_l$ is very long further it will be almost impossible to get a fully time-converged solution. One reason is that one run for $t=740$ in Fig. 11

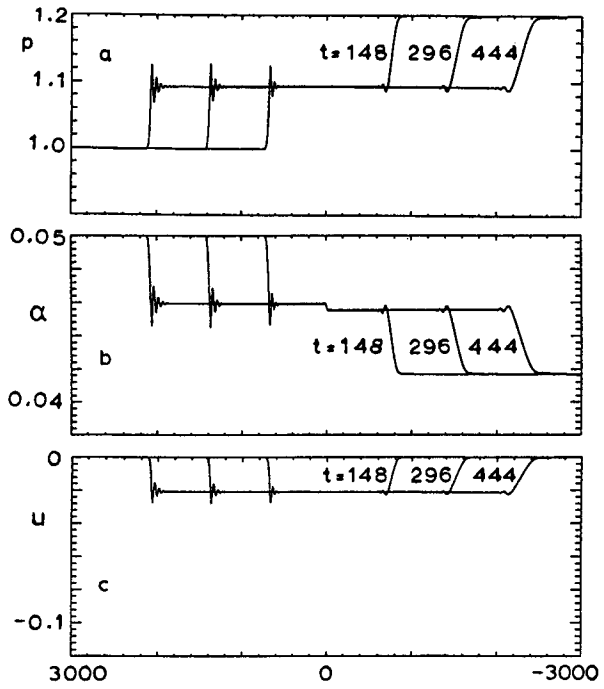

Fig. 12 Time evolution of flow field for mixture model after rupture of a diaphragm for $p_2/p_0=1.2$ and $n=1.0$; a pressure, b void fraction, c mixture velocity.

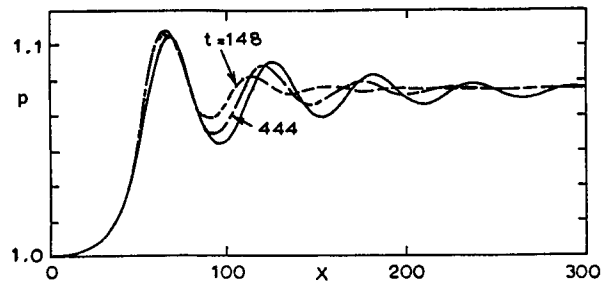

Fig. 13 Time-convergeny of shock front for mixture model for $p_2/p_0=1.2$ and $n=1.0$; ----- unsteady shock at $t=148$, ---- unsteady shock at $t=444$, —— stationary shock for $p_1/p_0=1.0933$.

required more than two hours of computing time on the supercomputer.

For comparison, a numerical solution to the mixture model ($u_l=u_g=u$) for the same initial conditions as those for the previous solutions was performed and the results are shown in Fig. 12a to 12c. Obviously the shock front is very oscillatory and the amplitude of the oscillation becomes larger with increasing time in the early stage of the evolution, but for a long time it asymptotically tends to converge. In this case, the central part of the profiles remains almost constant for $t>148$ and we can find the conditions denoted by the subscript 1 used in the calculation of stationary shocks. For example, the present result yields $p_1/p_0=1.0933$ for $p_2/p_1=1.2$. To show more clearly the time-convergency of the shock front, the unsteady pressure profiles for $p_2/p_0=1.2$ are compared with a stationary shock for $p_1/p_0=1.0933$ in Fig. 13. We can see a satisfactory time-convergency of the unsteady shock with the corresponding stationary shock. This is very important numerically as well as theoretically. The steady and unsteady shocks were calculated with comletely different numerical schemes. In spite of this, the good agreement between the stationary shock and the unsteady shock for large t suggests sufficient reliability and accuracy of the present numerical schemes and the results.

Finally, one more important finding is described here. By comparison between the results in Figs. 10a and 12a, we can clearly recognize that the shock propagation to the left and the rarefaction wave propagating to the right in Fig. 10a are appreciably faster than those in Fig. 12a. This result is quite consistent with a theoretical prediction that the speed of pressure waves in the bubbly liquid for $u_l \neq u_g$ is faster than that for $u_l=u_g$.

5. Conclusion

Weak shock waves in a bubbly liquid were calculated numerically. Results for stationary shocks indicate that the relative translational motion of bubbles affects appreciably the whole shock structure. Three types of shock structure are found numerically for a mixture with relative translational motion of bubbles. It is interesting that the translational motion of bubbles cooperates with the dissipations due to the thermal conduction in the gas and acoustic radiation in the liquid to suppress effectively the oscillatory behaviour near the shock front.

Shock tube problems have also been solved numerically. For the mixture model, it was confirmed that an unsteady shock same as above approaches asymptotically with time the corresponding stationary shock. This situation is substantially the case even for a mixture with relative translational motion of bubbles. The shock layer, however, becomes very long and then a large amount of time or a long distance will be needed for the shock to be stationary after the rupture of a diaphragm. This suggests that it is very difficult to realize a stationary shock experimentally. The shock speed depends appreciably on the relative motion of the bubbles. Experimentally it is absolutely necessary to measure the shock speed very carefully and accurately to confirm the steadiness or unsteaduness of the realized shock in the laboratory.

Appendix A. Hyperbolicity of the system

Although the hyperbolicity of the system was discussed in the previous paper[9], here we discuss it more precisely and prove that a slight modification is needed in the previous result.

We define a function $F(X)$ by

$$F(X)=X^4+3\varepsilon X^3+\left\{2\varepsilon^2-\frac{\rho_g D_M}{k}-C^2\left[1+\frac{\alpha_0}{k\rho_g}(1-\alpha)\right]\right\}X^2-\varepsilon C^2\left(1+\frac{1-\alpha}{2k}\right)X$$
$$+\frac{1-\alpha}{k}C^2\left(\rho_g D_M-\frac{\varepsilon^2}{2}\right), \tag{A 1}$$

with which Eq. (45) can be written as

$$F(X)=0. \tag{A 2}$$

For a solution X to the above equation, the left and the right eigenvectors $l=(l_1, l_2,$

l_3, l_4) and $r^T=(r_1, r_2, r_3, r_4)$ are obtained as

$$
\begin{aligned}
l_1&=\frac{k\,a}{1-\alpha}(X+\varepsilon)+\frac{\rho_g}{(1-\alpha)C^2}(X+u_l)\left[D_M+\frac{\alpha_0}{{\rho_g}^2}(1-\alpha)C^2\right]\\
&\quad-\frac{k}{(1-\alpha)C^2}(X^2+3\varepsilon X+2\varepsilon^2)(X+u_l),\\
l_2&=-\frac{k}{\rho_g}(X+2\varepsilon),\\
l_3&=\frac{k}{(1-\alpha)C^2}(X^2+3\varepsilon X+2\varepsilon^2)-\frac{\rho_g}{(1-\alpha)C^2}\left[D_M+\frac{\alpha_0}{{\rho_g}^2}(1-\alpha)C^2\right],\\
l_4&=1,
\end{aligned}
\tag{A 3}
$$

$$
\begin{aligned}
r_1&=1,\\
r_2&=\frac{\rho_g}{(1-\alpha)C^2}[X^2-(1-\alpha)C^2],\\
r_3&=-(X-u_l),\\
r^4&=-\frac{\varepsilon}{2}(4k-1)+\frac{ka X}{1-\alpha}-\frac{k}{(1-\alpha)C^2}(X+\varepsilon)[X^2-(1-\alpha)C^2].
\end{aligned}
\tag{A 4}
$$

Since Eq. (A 2) has four real distinct roots under the condition (46), we have four left eigenvectors and the corresponding four right eigenvectors. Denoting any two solutions to Eq. (A 2) by X and Y, the left eigenvector l for X and the right eigenvector r for Y satisfy

$$
\begin{aligned}
-\frac{(1-\alpha)C^2}{k}lr&=(X+Y)(X^2+Y^2)+3\varepsilon(X^2+XY+Y^2)\\
&\quad+\left\{2\varepsilon^2-\frac{\rho_g D_M}{k}-C^2\left[1+\frac{\alpha_0}{k\rho_g}(1-\alpha)\right]\right\}(X+Y)\\
&\quad-\varepsilon C^2\left(1+\frac{1-\alpha}{2k}\right).
\end{aligned}
\tag{A 5}
$$

For $X\neq Y$, we have a relation by making use of $F(X)-F(Y)=0$

$$
\begin{aligned}
\varepsilon C^2\left(1+\frac{1-\alpha}{2k}\right)&=(X+Y)(X^2+Y^2)+3\varepsilon(X^2+XY+Y^2)\\
&\quad+\left\{2\varepsilon^2-\frac{\rho_g D_M}{k}-C^2\left[1+\frac{\alpha_0}{k\rho_g}(1-\alpha)\right]\right\}(X+Y),
\end{aligned}
$$

with which we have $lr=0$. Next for $X=Y$, Eq. (A 2) becomes

$$-\frac{(1-\alpha)C^2}{k}lr=4X^3+9\varepsilon X^2+2\left\{2\varepsilon^2-\frac{\rho_g D_M}{k}\right.$$
$$\left.-C^2\left[1+\frac{\alpha_0}{k\rho_g}(1-\alpha)\right]\right\}X-\varepsilon C^2\left(1+\frac{1-\alpha}{2k}\right) \tag{A 6}$$

The right hand side is equal to dF/dX which is not zero at X satisfying $F(X)=0$, because $F(X)=0$ has four real distinct roots. This means that the system has four linearly independent eigenvectors and that the system is totally hyperbolic. In the previous paper, it was concluded that the system is hyperbolic if $F(X)=0$ has four real roots, which is not sufficient. More strictly Eq. (45) must have four distinct real roots for the system to be hyperbolic.

It is also important to describe the fact that the solution X in the expansion series with respect to small velocity slip ε in the previous paper[9] is not appropriate, because the convergence of the series is not good. So this time the solution to $F(X)=0$ is solved purely numerically.

Appendix B. Governing equations for the mixture model

For the mixture model, Eqs. (1) to (3), (5), (7), (10) and (11) are rearranged as follows:

$$\frac{\partial q}{\partial t}+\frac{\partial f}{\partial x}=h, \tag{B 1 a}$$
$$q^T=[(1-\alpha),\ \alpha\rho_g,\ (1-\alpha)u], \tag{B 1 b}$$
$$f^T=[(1-\alpha)u,\ \alpha\rho_g u,\ p_g+(1-\alpha)u^2], \tag{B 1 c}$$
$$h^T=(0,\ 0,\ W), \tag{B 1 d}$$
$$A=\frac{\partial f}{\partial q}=\begin{bmatrix} 0 & 0 & 1 \\ -\dfrac{\alpha}{1-\alpha}\rho_g u & u & \dfrac{\alpha}{1-\alpha}\rho_g \\ n\Gamma\dfrac{\rho_g{}^n}{\alpha}-u^2 & n\Gamma\dfrac{\rho_g{}^{n-1}}{\alpha} & 2u \end{bmatrix}, \tag{B 2}$$
$$\frac{\rho_g{}^{-2/3}}{3\alpha(1-\alpha)}\frac{\partial^2 W}{\partial x^2}+\left\{\frac{\partial}{\partial x}\left[\frac{\rho_g{}^{-2/3}}{3\alpha(1-\alpha)}\right]+\frac{\rho_g{}^{-2/3}}{3\alpha(1-\alpha)^2}\left(\frac{\partial\alpha}{\partial x}\right)\right\}\frac{\partial W}{\partial x}$$
$$+\left\{\frac{\partial}{\partial x}\left[\frac{\rho_g{}^{-2/3}}{3\alpha(1-\alpha)^2}\left(\frac{\partial\alpha}{\partial x}\right)\right]-1\right\}W-\frac{\rho_g{}^{-2/3}}{3\alpha(1-\alpha)}\frac{\partial^3 p_g}{\partial x^3}-\left\{\frac{\partial}{\partial x}\left[\frac{\rho_g{}^{-2/3}}{3\alpha(1-\alpha)}\right]\right.$$

$$+\frac{\rho_g^{-2/3}}{3\alpha(1-\alpha)^2}\left(\frac{\partial\alpha}{\partial x}\right)\Big\}\frac{\partial^2 p_g}{\partial x^2}-\frac{\partial}{\partial x}\left[\frac{\rho_g^{-2/3}}{3\alpha(1-\alpha)^2}\left(\frac{\partial\alpha}{\partial x}\right)\right]\frac{\partial p_g}{\partial x}$$
$$-\frac{1}{9}\frac{\rho_g^{-2/3}}{\alpha^2}\left(\frac{\partial u}{\partial x}\right)\left(\frac{\partial^2 u}{\partial x^2}\right)-\frac{1}{18}\frac{\partial}{\partial x}\left(\frac{\rho_g^{-2/3}}{\alpha^2}\right)\left(\frac{\partial u}{\partial x}\right)^2$$
$$+\frac{4\Psi}{3Re}\left[\frac{1}{\alpha}\frac{\partial^2 u}{\partial x^2}-\frac{1}{\alpha^2}\left(\frac{\partial\alpha}{\partial x}\right)\left(\frac{\partial u}{\partial x}\right)\right]=0, \tag{B 3}$$

$$p=p_g-\frac{\rho_g^{-2/3}}{3\alpha(1-\alpha)}\frac{\partial W}{\partial x}-\frac{\rho_g^{-2/3}}{3\alpha(1-\alpha)^2}\left(\frac{\partial\alpha}{\partial x}\right)W$$
$$+\frac{\rho_g^{-2/3}}{3\alpha(1-\alpha)}\frac{\partial p_g}{\partial x^2}+\frac{\rho_g^{-2/3}}{3\alpha(1-\alpha)^2}\left(\frac{\partial\alpha}{\partial x}\right)\frac{\partial p_g}{\partial x}+\frac{1}{18}\frac{\rho_g^{-2/3}}{\alpha^2}\left(\frac{\partial u}{\partial x}\right)^2$$
$$-\frac{4\Psi}{3Re}\frac{1}{\alpha}\left(\frac{\partial u}{\partial x}\right), \tag{B 4}$$

$$p_g=\Gamma\rho_g{}^n. \tag{B 5}$$

Eigenvalues ν of the matrix A are easily obtained as

$$\nu=u+C,\ u,\ u-C, \tag{B 6}$$

where

$$C^2=\frac{n\Gamma\rho_g{}^n}{\alpha(1-\alpha)}=\frac{np_g}{\alpha(1-\alpha)}. \tag{B 7}$$

References

1) I. J. Campbell and A. S. Pitcher, "Shock Waves in Liquid Containing Gas Bubbles," Proc. Royal. Soc. (London) A243, 534 (1958).
2) R. B. Eddington, "Investigation of Supersonic Phenomena in a Two-Phase (Liquid-Gas) Tunnel," AIAA Journal 8, 65 (1970).
3) A. Crespo, "Sound and Shock Waves in Liquids Containing Bubbles," The Physics of Fluids 12, 2274 (1969).
4) L. Noordzij, "Shock Waves in Bubbly-Liquid Mixtures," Proc. IUTAM Symp. on Nonsteady Flow of Water at High Speeds, ed. L. I. Sedov & Yu-Stepanov, Moscow: Nauka, 369 (1973).
5) L. Noordzij and L van Wijngaarden, "Relaxation effects, caused by relative motion, on shock waves in gas-bubble/liquid mixtures," J. Fluid Mech. 66, part. 1, 115 (1974).
6) M. J. Tan and S. G. Bankoff, "Propagation of pressure waves in bubbly mixtures," Physics of fluids 27, 1362 (1983).
7) A. I. Ivandaev, "Numerical Simulation of One-Dimensional Shock Waves in Bubbly Liquids," Proc. Symp. on Shock Waves, Japan '90, Tokyo, 443 (1990).
8) A. E. Beylich and Ali Gülhan, "On the structure of nonlinear waves in liquid with gas bubbles,"

Phys. Fluids A2, 1412 (1990).

9) R. Ishii, Y. Umeda, S. Murata and N. Shishido, " Bubbly flows through a converging-diverging nozzle, " Physics of fludis A5, 1630 (1993).
10) L. van Wijngaarden, " Hydrodynamic interaction between gas bubbles, " J. Fluid Mech. 77, 27 (1976).
11) G. K. Batchelor, " A new theory of a uniform fluidized bed, " J. Fluid Mech. 193, 75 (1988).
12) A. Prosperetti, " The thermal behaviour of oscillating gas bubbles, " J. Fluid Mech. 222, 587 (1991).
13) C. Devin, Jr., " Survey of Thermal Radiation, and Viscous Damping of Pulsating Air Bubbles in Water, " J. Acoust. Soc. Amer. 31, 1654 (1959).
14) S. R. Chakravarthy, & S. Osher, " A new class of high accuracy TVD schemes for hyperbolic conservation laws, " AIAA paper 85-0363 (1985).
15) R. Ishii, N. Hatta, Y. Umeda and M. Yuhi, " Supersonic gas-particle two-phase flow around a sphere, " J. Fluid Mech. 221, 453 (1990).
16) A. Prosperetti and L. van Wijngaarden, " On the characteristics of the equation of motion for a bubbly flow and the related problem of critical flow, " J. Engng. Math. 10, 153 (1976).
17) L. van Wijngaarden, " One-Dimensional Flow of Liquids Containing Small Gas Bubbles, " Annual Review of Fluid Mechanics 4, 369 (1972).